Uncovering the hidden ground state of green fluorescent protein

John T. M. Kennis[†‡§], Delmar S. Larsen[†‡], Ivo H. M. van Stokkum[†‡], Mikas Vengris[†], Jasper J. van Thor[¶], and Rienk van Grondelle[†]

[†]Department of Biophysics, Faculty of Sciences, Vrije Universiteit Amsterdam, De Boelelaan 1081, Amsterdam 1018HV, The Netherlands; and [¶]Laboratory of Molecular Biophysics, University of Oxford, Oxford OX1 3QU, United Kingdom

Edited by Martin Chalfie, Columbia University, New York, NY, and approved November 11, 2004 (received for review June 15, 2004)

The fluorescence properties of GFP are strongly influenced by the protonation states of its chromophore and nearby amino acid side chains. In the ground state, the GFP chromophore is neutral and absorbs in the near UV. Upon excitation, the chromophore is deprotonated, and the resulting anionic chromophore emits its green fluorescence. So far, only excited-state intermediates have been observed in the GFP photocycle. We have used ultrafast multipulse control spectroscopy to prepare and directly observe GFP's hidden anionic ground-state intermediates as an integral part of the photocycle. Combined with dispersed multichannel detection and advanced global analysis techniques, the existence of two distinct anionic ground-state intermediates, I_1 and I_2, has been unveiled. I_1 and I_2 absorb at 500 and 497 nm, respectively, and interconvert on a picosecond timescale. The I_2 intermediate has a lifetime of 400 ps, corresponding to a proton back-transfer process that regenerates the neutral ground state. Hydrogen/deuterium exchange of the protein leads to a significant increase of the I_1 and I_2 lifetimes, indicating that proton motion underlies their dynamics. We thus have assessed the complete chain of reaction intermediates and associated timescales that constitute the photocycle of GFP. Many elementary processes in biology rely on proton transfers that are limited by slow diffusional events, which seriously precludes their characterization. We have resolved the true reaction rate of a proton transfer in the molecular ground state of GFP, and our results may thus aid in the development of a generic understanding of proton transfer in biology.

hidden reaction intermediates | multipulse control spectroscopy | proton transfer | ultrafast spectroscopy

In the last decade, GFP has become the fluorescent label of choice in cell biology and many other research fields (1). Despite GFP's obvious significance for biological investigation, some key molecular processes that define its fluorescence characteristics have remained poorly understood. This concerns in particular the dynamic protonation state of the chromophore and its nearby protein environment: GFP absorbs primarily in the near UV but fluoresces in the green. It is widely believed that the large shift of the emission to longer wavelengths after near-UV absorption is caused by a deprotonation reaction in the excited state of the neutral chromophore (2). The absorption spectrum of GFP (Fig. 1 *Upper*, blue line) exhibits a main absorption band near 400 nm, belonging to state A, and a minor band at 480 nm, belonging to state B (1). A corresponds to a state of the protein wherein the chromophore assumes a neutral form and B to a state with a deprotonated anionic chromophore. Upon excitation of the A band with near-UV light, the chromophore deprotonates on a picosecond timescale, and subsequent proton transport occurs, most likely via a hydrogen-bonded network that involves an internal water molecule (W25), a serine residue (S205), and a terminal proton acceptor, an ionized glutamate (E222), as indicated in Fig. 1 *Lower* (3). The thus-formed intermediate state, with a deprotonated anionic chromophore and a protonated neutral glutamate, is generally referred to as I* and is the emitting state of GFP. The fluorescence spectrum of GFP upon excitation at 400 nm is also shown in Fig. 1 *Upper* (green line). The B state is not part of the fluorescence photocycle studied here, and it has been proposed that it is irreversibly formed with a low quantum efficiency by decarboxylation of E222 (4).

An anionic ground-state species, which has been labeled I, can be stabilized and photoconverted back to A at cryogenic temperature (5). It was postulated that the molecular ground state of the chromophore in this anionic form acts as an intermediate in the GFP photocycle (2, 5–8). However, with time-resolved spectroscopy, only the excited states A* and I* of GFP could be detected (9), and the molecular nature and dynamics of any ground-state intermediate remained elusive.

Here, we aim to directly measure the proton transfer dynamics in GFP. To this end, we have applied multipulse control spectroscopy to GFPuv, a widely used GFP mutant (10). GFPuv exhibits the same photophysical properties as wild-type GFP but has better solubility in water. Moreover, it shows a diminished B band, allowing for a higher selectivity of A band excitation with near-UV light. Multipulse spectroscopy can be used to control and influence the course of reactions as they evolve, and its power lies in the ability to selectively remove or transfer the population of transient species with carefully timed laser pulses (11–13). We have recently expanded this technique by combining it with broad-band spectral probing and elaborate global analysis techniques, enabling us to disentangle complex branched reaction schemes (14–18). In this work, we describe the direct observation of the hidden anionic ground state of GFP as an integral part of the photocycle, revealed through the use of multipulse spectroscopy in combination with global analysis techniques. We report the actual existence of two distinct anionic ground-state intermediates, show their absorption spectra and the dynamics by which they interconvert, and resolve the proton back-transfer process that regenerates the neutral ground state.

Materials and Methods

Experimental Procedures. GFPuv (including surface exposed mutations F99S, M153T, and V163A) was prepared as described (19) and dissolved in a 20-mM H_2O Tris·HCl buffer (pH 8.0). The absorbance was adjusted to 0.3 per mm at 400 nm. For the hydrogen/deuterium (H/D) exchange experiments, GFP was dissolved in a 20-mM D_2O Tris·HCl buffer at [pD 8.1; pD = $-\log [D^+]$ ($[D^+]$, the deuterium ion concentration)]. The H_2O to D_2O buffer exchange was conducted 2 days before the experiments at room temperature to ensure efficient H/D exchange of the protein. The sample was loaded in a flow system of 2-ml volume and pumped through a flow

This paper was submitted directly (Track II) to the PNAS office.

Abbreviations: SADS, species-associated difference spectra; H/D, hydrogen/deuterium.

[‡]J.T.M.K., D.S.L., and I.H.M.v.S. contributed equally to this work.

[§]To whom correspondence should be addressed. E-mail: j.kennis@few.vu.nl.

www.pnas.org/cgi/doi/10.1073/pnas.0404262102

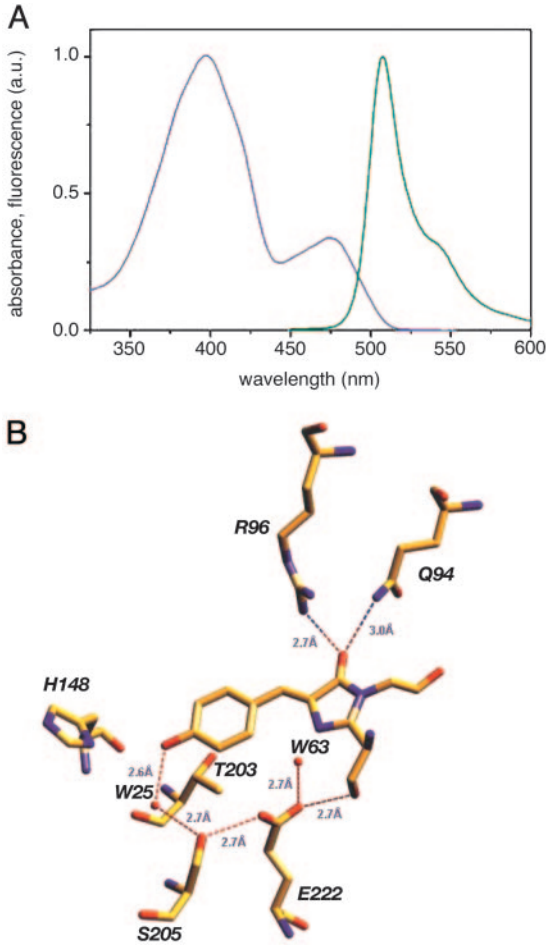

Fig. 1. Absorption and fluorescence spectra and structural features of GFP. (*A*) Absorption (blue line) and fluorescence (green line) spectrum of GFP. (*B*) Structural arrangement of chromophore-binding pocket in GFP in the neutral ground-state A. The coordinates were taken from Protein Data Bank entry 1GFL [Yang *et al.* (3)].

cuvette of 1-mm path length. The pump–probe setup has been described in detail (20) and has been modified to include an additional pulse (15, 17). The basis of the system is a 1-kHz amplified Ti:sapphire laser system (Coherent Radiation, Mountain View, CA; BMI, Evry, France) delivering 450-μJ 60-fs 800-nm pulses. The multipulse results presented here involve intense laser pulses at two wavelengths, 400 and 540 nm. The 400-nm pump pulses were generated by frequency doubling a portion of the amplified 800-nm light, whereas the 540-nm dump pulses were generated with a noncollinear optical parametric amplifier. The white-light continuum, used as the broad-band probe pulse, was produced by focusing a weak 800-nm beam into a CaF_2 crystal. The sample was pumped through a 1-mm quartz flow cell. The polarizations of the pump and dump pulses were set parallel to each other and at a magic angle (54.7°) to the probe pulse. Pump and dump pulse intensities of ≈200 nJ per pulse were used. The pump and dump beam spot size at the focus was ≈300 μm, and a 125-fs instrument response function in the time domain was estimated.

Data Analysis. The collected data were fitted by using the global analysis technique described in *Supporting Text* and Fig. 6, which are published as supporting information on the PNAS web site, and as recently reviewed in ref. 18. Underlying this analysis is the

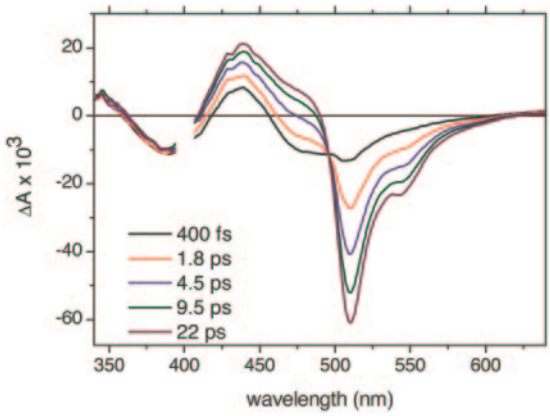

Fig. 2. Time-resolved absorbance difference spectra recorded in GFP upon excitation at 400 nm at the time delays indicated.

construction of a connectivity scheme, which describes how transient states are linked (e.g., in series, parallel, or an admixture of both). The target analysis gives several important benefits. It allows the experimentalist to quantify the results in terms of microscopic rate constants and the species-associated difference spectra (SADS) for different compartments. Moreover, it reduces the unwieldy set of multipulse and conventional pump–probe data (both 2D surfaces) into the smaller set of SADS. In conjunction with the underlying connectivity scheme and the relatively small number of more precisely estimated rate constants, this greatly simplifies the interpretations of the complex data.

Results and Discussion

Conventional Pump–Probe Spectroscopy. In Fig. 2, time-resolved spectra recorded on GFP are shown with excitation at 400 nm and broad-band white-light probing. The first spectrum (black line), taken at a delay of 400 fs, exhibits a ground-state bleaching near 400 nm, an excited-state absorption band at 440 nm, and a broad stimulated emission band ranging from 450 to 550 nm. This stimulated emission can primarily be assigned to the excited state of the neutral chromophore, A*. At progressively increasing time delays, a pronounced stimulated emission band with a maximum amplitude ≈509 nm and a shoulder at 545 nm develops. The intensity of the stimulated emission signal near 509 nm is a direct measure of the population of I*, and these results indicate formation of I* on a picosecond timescale, which corresponds to a deprotonation reaction of the phenolic oxygen of the chromophore. Because the amplitude of the stimulated emission band at 509 nm is significantly larger than the ground-state bleach near 400 nm, these data also indicate that the emission dipole strength of the I* species is significantly larger than that of A*. Concomitant with the rise of stimulated emission, the excited-state absorption around 440 nm increases, indicating that, like A*, I* has a pronounced excited-state absorption in this spectral region. The transient absorption signal then slowly decays to zero amplitude on a nanosecond timescale (spectra not shown). These dynamics are also reflected in Fig. 3*A*, where the kinetic trace probed at 509 nm is shown (blue line). The trace shows little signal at early times after excitation, and on a timescale of several picoseconds, the stimulated emission signal rises to maximum (negative) amplitude. The emission signal subsequently decays to zero in ≈3 ns, which corresponds mainly to radiative decay to the ground state (8, 21). A global analysis of the time-resolved data in terms of a sum of exponentials is presented in *Supporting Text*.

BIOPHYSICS

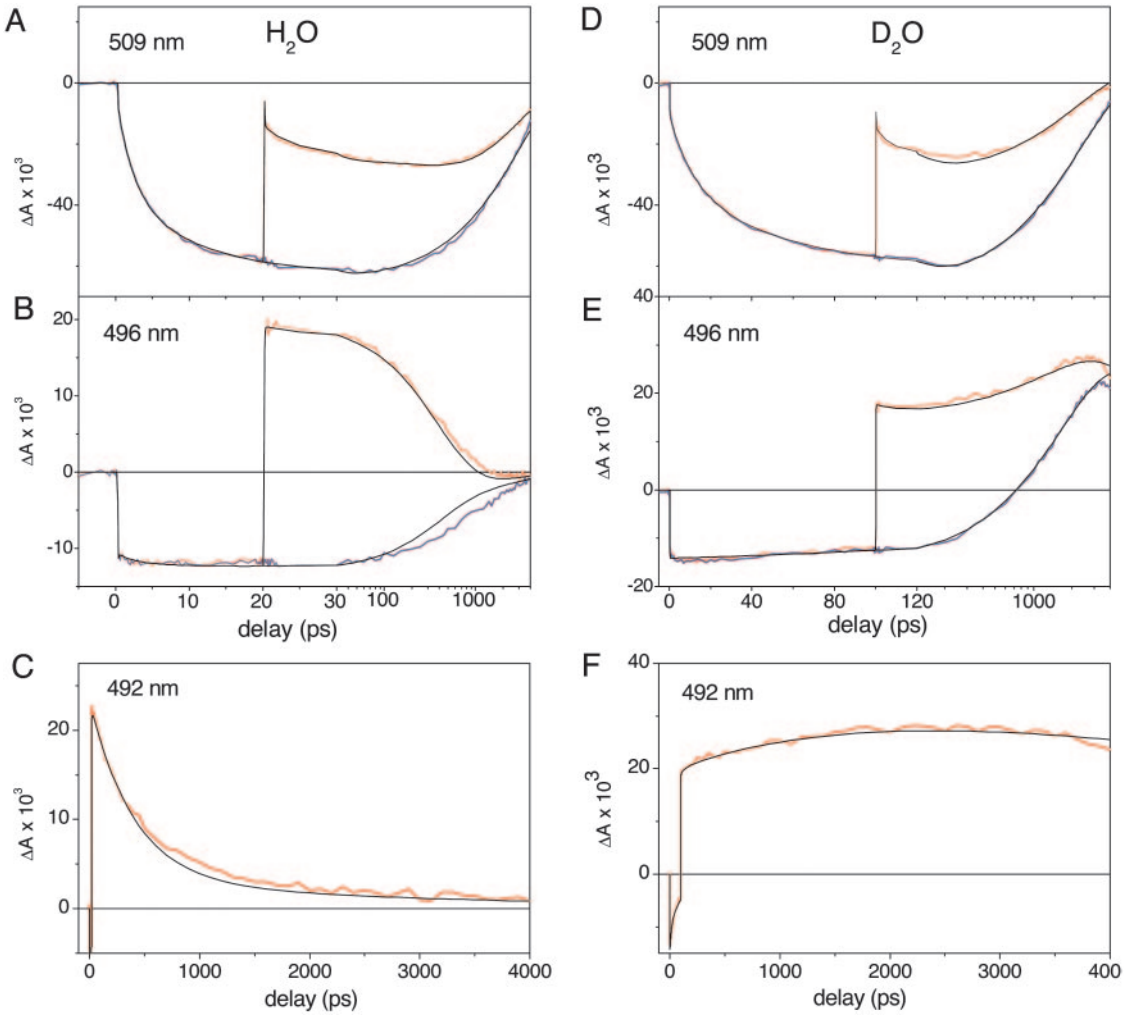

Fig. 3. Transient absorption traces recorded in GFP upon excitation at 400 nm in H_2O and D_2O, in the presence or absence of a dump pulse at 540 nm. (*A–C*) Transient absorption trace of GFP at 509 (*A*), 496 (*B*), and 492 (*C*) nm in a H_2O buffer in the absence (blue curve) and presence (red curve) of a dump pulse at 540 nm at 20-ps delay. The black lines denote the result of the global fitting procedure. The time axis is linear up to 30 ps, logarithmic thereafter in *A* and *B*, and linear throughout (*C*). (*D–F*) Transient absorption trace at 509 (*D*), 496 (*E*), and 492 (*F*) nm with excitation of GFP in a D_2O buffer in the absence (blue curve) and presence (red curve) of a dump pulse at 540 nm at 100-ps delay. The time axis is linear up to 120 ps, logarithmic thereafter in *D* and *E*, and linear throughout (*F*).

Application of Multipulse Control Spectroscopy to GFP. The stimulated emission process can be used to transfer population on a femtosecond timescale from the excited state to the ground state: with an intense pulse resonant with the stimulated emission, a portion of the excited-state population can be deexcited or "dumped" to the ground state (11, 12, 22). In the case of GFP, this is achieved by applying an additional green pulse in the time-resolved experiment. We have used this property to uncover ground-state intermediates in the GFP photocycle that so far remained hidden. The red curve in Fig. 3*A* shows the kinetic trace at 509 nm in the presence of a short dump pulse at 540 nm, which overlaps with a shoulder of GFP's fluorescence spectrum and is fired 20 ps after the 400-nm excitation flash. Up to 20 ps, the trace overlaps with an unmodified, e.g., without dump-pulse transient absorption trace. At 20 ps, a sudden decrease of the stimulated emission signal shows that the excited-state population has decreased as a result of the action of the dump pulse. In Fig. 3*B*, the corresponding kinetic traces at 496 nm have been depicted. The red curve denotes the transient absorption signal at 496 nm in the presence of the dump pulse. We observe that at 20 ps, a large induced absorption appears. This indicates that, concomitant with the depletion of the excited state as a result of the action of the dump pulse, a product species is formed that absorbs at 496 nm. This species corresponds to the ground state of the deprotonated chromophore, I, and this experiment thus clearly demonstrates a ground-state intermediate in the photocycle of GFP. Fig. 3*C* shows the kinetic trace at 492 nm, where I* shows an isosbestic point and does not exhibit any absorbance changes. At this wavelength, the signals almost exclusively represent the dynamic behavior of the ground state species I (red curve). We observe that, after its formation by the dump pulse, the I state disappears rapidly; the smooth curve represents a fit of the data with a single exponential decay of 400 ps, according to a global analysis procedure described below and in *Supporting Text*. Without the dump pulse, the I state remains invisible, because it decays ≈10 times faster than it is formed.

To illustrate the spectral evolution induced by the dump pulse, time-resolved spectra at selected delays are shown in Fig. 4 in the presence (dashed lines) and absence (solid lines) of the dump pulse at 20 ps. As can be seen from the difference spectrum taken at a delay of 22 ps (i.e., 2 ps after the dump pulse, Fig. 4*A*), the stimulated emission band of I* from 509 to 600 nm has been

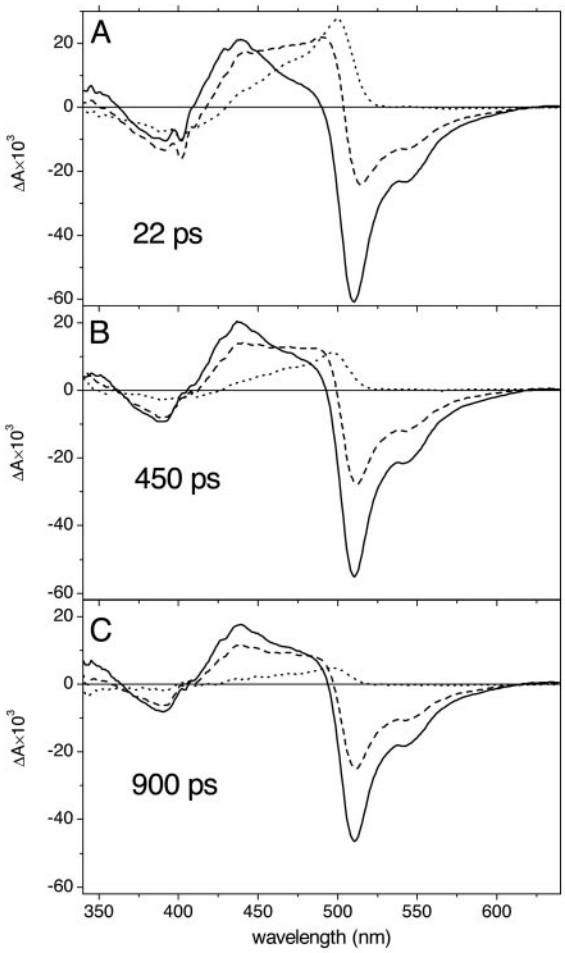

Fig. 4. Time-resolved absorbance difference spectra recorded on GFP at the delays indicated on excitation at 400 nm in the absence (solid line) and presence (dashed line) of a dump pulse at 540 nm, fired 20 ps after initial excitation. The dotted lines denote a double-difference spectrum, in which a fraction of 0.57 of the undumped spectrum is subtracted from the dumped spectrum, and denote the pure difference spectra corresponding to the anionic ground-state I. The time-resolved spectra were taken at delays of 22 (*A*), 450 (*B*), and 900 (*C*) ps.

significantly depleted. Moreover, a pronounced new absorption band near 500 nm is observed in the dumped spectrum, along with a red-shift of the isosbestic point (at 492 nm in the undumped spectrum) by 15 nm, indicating formation of the ground-state species upon dumping. Thus, the dumped spectrum is a superposition of the excited state species I* and the newly formed ground-state species I. To assess the spectral properties of the ground-state species I, the difference spectrum of I* was scaled by a factor of 0.57 (to reflect that an estimated fraction of 0.43 was dumped to the ground state) and subtracted from the dumped spectrum. The resulting double-difference spectrum (dotted line) corresponds to the "pure" absorption of I. At subsequent delays of the probe pulse (450 and 900 ps, Fig. 4 *B* and *C*), the absorption feature near 500 nm decreases significantly and the dumped spectrum starts to resemble the undumped spectrum, indicating that the newly formed ground-state species indeed has a significantly shorter lifetime than I*.

H/D Exchange Effects on the Photocycle of GFP. To investigate whether the dump-induced ground-state dynamics are related to proton transfer processes or other phenomena (e.g., vibrational relaxation), we have conducted the same experiment on GFP dissolved in D_2O. Fig. 3 *D* and *E* show the kinetic traces at 509 and 496 nm in the presence (red line) and absence (blue line) of a dump pulse, respectively. The rise of the stimulated emission at 509 nm is ≈6 times slower than in the experiment in H_2O (Table 1 and Fig. 3 *A* and *D*), which agrees with earlier time-resolved fluorescence experiments (2). For this reason, the dump pulse was applied after 100 rather than 20 ps. As in GFP in H_2O, a pronounced absorption of the I species is induced by the dump pulse (Fig. 3*E*). However, as can be seen in Fig. 3*F*, the I species hardly decays on the timescale of our experiment, in contrast to GFP in H_2O. In accordance with this, due to the decreased rate of the decay of I in D_2O, it also becomes populated after several nanoseconds in the absence of the dump pulse (Fig. 3*E*, blue line). These features also become apparent in Fig. 7, which is published as supporting information on the PNAS web site, where time-resolved multipulse spectra of GFP in D_2O at selected delays are presented.

Identification of Ground-State Intermediates: Target Analysis. The time-resolved data shown in Figs. 3 and 4 reveal the existence of transient ground-state intermediates in the photocycle of GFP. However, from the data itself, it is not straightforward to extract the spectral and temporal information necessary to assess the precise molecular events that underlie the GFP photophysics. To identify the intermediate states in the GFP photocycle and determine their dynamic behavior, we globally analyzed the time-resolved data with a multipulse target analysis (18). We imposed a photocycle scheme as depicted in Fig. 5 *Upper*, along with a qualitative outline of the potential energy surfaces that govern proton motion in the protein. The kinetic scheme encompasses the known previously identified states in GFP: the ground-state A with the neutral chromophore, the excited neutral state A*, and the deprotonated excited state I*. Following the work by Chattoraj *et al.* (2), a biexponential decay of A* into I* was assumed. The model is simultaneously fitted to the conventional transient absorption and the multipulse data. The former is described by assuming a 3-ns lifetime for I*, whereas for the multipulse data, a fraction of the I* population is transferred instantaneously to a ground state species at the dump time. Moreover, it was required that the scheme described the dynamics of GFP in H_2O as well as in D_2O with similar difference spectra for the intermediates. Global analysis of the multipulse experiments indicated two distinct timescales accompanied by

Table 1. Time constants of the spectral evolution of GFP in H_2O and D_2O as they result from a target analysis of the conventional and multipulse transient absorption data

	Dump time, ps	A*→I*, ps	I*→I_1, ns	I_1→I_2, ps	I_2→A
GFP-H_2O	20	2.2 (49%) 11.1 (51%)	3.0	3	400 ps
GFP-D_2O	100	12 (42%) 69 (58%)	3.1	7	5 ns
Kinetic isotope effect*		≈6	–	≈2	12

*The kinetic isotope effect of H/D exchange on the various reaction steps.

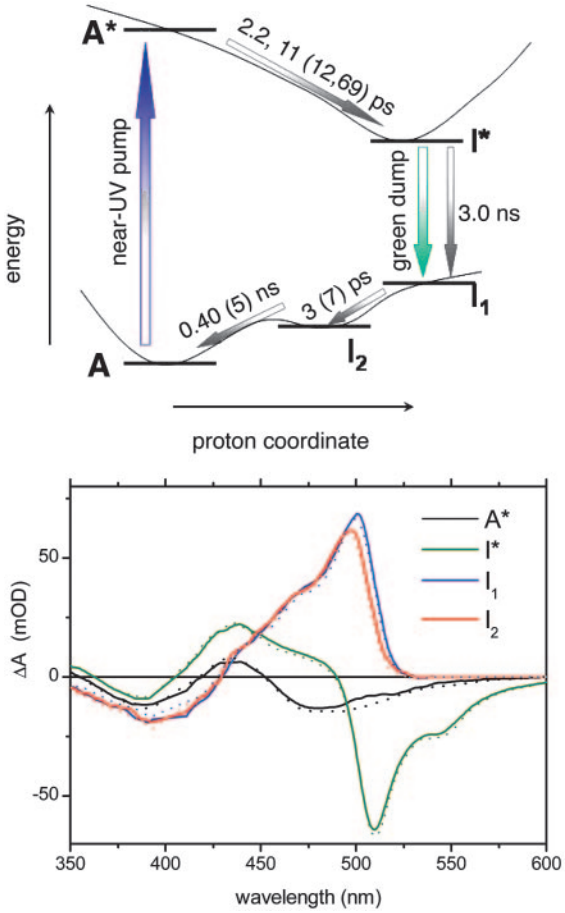

Fig. 5. Photocycle scheme of GFP and SADS of the involved GFP transient states. (*Upper*) Kinetic scheme and potential energy level surfaces representing the photocycle of GFP, to fit the multipulse and traditional transient absorption data of GFP in H_2O and D_2O. The time constants by which the states evolve into one another as estimated from the target analysis have been indicated at the arrows, with the values in parentheses representing those obtained for D_2O. (*Lower*) SADS of A* (black), I* (green), I_1 (blue), and I_2 (red) species relative to the A state that result from a target analysis of the time-resolved spectra recorded for GFP in H_2O (solid lines) and D_2O (dotted lines).

spectral evolution in the ground-state dynamics, in H_2O as well as in D_2O. This prompted us to include two ground-state intermediates, which we term I_1 and I_2. By means of the target analysis, the SADS of the states involved are estimated, along with the rate constants by which they evolve according to the kinetic scheme. On the basis of the spectrodynamic features that have been presented in Figs. 3, 4, and 7 and Fig. 8, which is published as supporting information on the PNAS web site, this kinetic scheme depicts the simplest representation of the photocycle of GFP. The resulting SADS of the photocycle intermediates with respect to state A have been depicted in Fig. 5 *Lower*. The difference spectra of A* and I* agree with those reported earlier (9) and resemble the raw time-resolved spectra at delays of 400 fs and 22 ps of Fig. 2, respectively. Notably, the difference spectra of all photocycle intermediates of GFP in D_2O (dashed lines) are practically the same as those in H_2O (solid lines), solidifying our kinetic modeling. The rate constants estimated from the target analysis on GFP in H_2O and in D_2O have been summarized in Table 1. Details of the target analysis procedure are given in *Supporting Text* and in Fig. 9, which is published as supporting information on the PNAS web site.

I_1 is formed on a femtosecond timescale by dumping I* with the green pulse. Therefore, I_1 has retained the protonation states of the chromophore and various residues in the I* state, i.e., a protonation of E222, and possibly with a rearranged hydrogen-bond network around the anionic chromophore. The difference spectrum of I_1 has a maximum at 500 nm, a shoulder at 475 nm, and a ground-state bleaching band around 400 nm. It is important to note that the steady-state absorption of A (Fig. 1 *Upper*) is negligible at wavelengths longer than 450 nm, which implies that, at these wavelengths, the SADS of I_1 corresponds to the "pure" absorption spectrum of I_1. It is very much mirror-symmetric with respect to the GFP fluorescence spectrum, with a similar energy spacing of $\approx$1,250 cm^{-1} between their main peaks (at 500 and 509 nm, respectively) and vibronic shoulders (at 470 and 540 nm, respectively).

I_1 lives for only 3 ps in H_2O and 7 ps in D_2O. With this time constant, I_1 evolves into I_2, which has a slightly blue-shifted absorption with a maximum at 497 nm, retaining the absorption properties of an anionic chromophore. This aspect of the GFP ground-state dynamics also becomes apparent upon close inspection of the raw time-resolved data, as shown in Fig. 8 *A* and *B*. At this point, it is not entirely clear what molecular properties underlie the difference between I_1 and I_2. The sensitivity to H/D exchange indicates that proton movement is involved in the I_1 to I_2 evolution, which suggests that a hydrogen-bond rearrangement has taken place. A dynamic blue shift of ground-state absorption on a picosecond timescale would be consistent with a vibrational cooling process in the ground state. However, one would not expect a pronounced H/D exchange effect on vibrational cooling in a protein environment. Note that the observation of multiple lifetimes in the ground-state evolution of GFP differs qualitatively from that in the excited state, because, in contrast to the excited state, an actual spectral evolution is associated with the ground-state dynamics.

The spectroscopic properties of I_1 and I_2 are different from GFP mutants, which have a stabilized anionic chromophore, like the S65T, enhanced GFP (EGFP), and Emerald GFP mutants. The absorption spectra of these mutants peak at 487–489 nm (1, 23) are significantly different from the absorption maximum of I_1 (500 nm) and I_2 (497 nm). Moreover, the fluorescence Stokes shift of I_1 (8 nm) is significantly smaller than in the S65T mutant (22 nm), EGFP (20 nm) and Emerald GFP (22 nm) (1). Interestingly, the spectrum of I_2 closely corresponds to a recently constructed GFP mutant, with alterations specifically designed to stabilize the I state of the chromophore that was observed in steady state (24).

In GFP in H_2O, I_2 evolves with a lifetime of 400 ps into the neutral A species, indicating that we have resolved the crucial back-shuttle of the proton to the anionic chromophore. The corresponding process in D_2O takes 5 ns, implying a kinetic isotope effect as large as a factor of 12. This unusually large kinetic isotope effect is unlikely to arise from a single proton transfer step in the hydrogen bond network that connects E222 to the chromophore. The most straightforward interpretation is that it arises from multiple proton transfers: in the I_2 state, the proton still resides on E222 and is transferred via S205 and the bound water to the anionic chromophore in 400 ps in H_2O and 5 ns in D_2O. Given the resemblance of I_2 to the cryotrapped I species reported earlier (5), it is very likely that they correspond to similar molecular species. It may be concluded that the back-shuttle process is thermally activated, as originally proposed by Creemers *et al.* (5) and indicated in the potential energy surface diagram of Fig. 5*A*.

In a recent molecular dynamics simulation study by Lill and Helms (25), the proton forward-transfer and back-shuttle processes were studied. It was found that the initial event of the back transfer entailed a reprotonation of the chromophore by the internal water on a timescale between 1 ps and 1 ns, followed by an extremely fast (<500 fs) concerted "backing up" of the

hydrogen-bonding network to reprotonate the internal water and deprotonate E222. These results suggest that the reprotonation of the anionic chromophore by the internal water molecule is rate-limiting for the overall reaction and occurs with the 400-ps time constant observed in the present study.

Proton Transfer in Biological Systems. Proton transfer is an important event in the functioning of proteins, whether involved in signal transduction, enzymatic reactions, or cell metabolism. Proton transfer through proteins often proceeds via a network of hydrogen-bonded amino acid side chains, by which it is not always necessary that a specific proton is physically transferred, but it may rather be the proton charge that is propagated through a chain of hydrogen-bonded molecules. In this sense, with its simple light-driven proton transfer reaction along a chain of a water molecule and two amino acids, GFP can be regarded as an attractive and compact model system to understand the basic principles of proton transfer in biological systems. Especially our observation of the proton back shuttle from the glutamic acid to the chromophore may yield important insights, because this reaction takes place in the molecular ground state, as does the vast majority of proton transfers in biology. We have determined the "true" intrinsic rate constant of ground-state proton transfer in a protein by moving the proton with the first-femtosecond pulse to a terminal acceptor, instantaneously switching the pK of the donor back to its original value, and then watching the proton migrate back. In particular, because we have demonstrated that intraprotein proton transfer processes in the ground state occur at ultrafast rates of <1 ns, these results may aid in the development of a generic understanding of proton transfer in biology like in respiratory and signaling pathways. In these systems, diffusional events from the aqueous solution to the molecular surface, which take $\approx 10^{-5}$ s at physiological pH (26), often limit the proton-transfer rate, obscuring a view of the actual proton transfer reaction.

Conclusion

In the recent past, the understanding of reactive processes in biology has benefited greatly from the application of time-resolved spectroscopic methods. However, biological reactions are generally so complex that slow rate-limiting events may often obscure reaction intermediates. These events may involve large-scale motions like protein diffusion in intermolecular signaling processes, but small-scale motions, like intramolecular proton or electron transfer (27), may also suffer from this limitation. These inherent properties of time-resolved spectroscopy preclude a complete understanding of fundamental processes in biology. In this work, we have overcome this problem. Through the use of multiple pulse-sequence schemes, we were able to initiate, halt, and reverse a proton transfer process within GFP and demonstrate hitherto unobserved transient ground-state molecular species. In combination with advanced global analysis methods, we have thus obtained a complete and detailed view of the proton transfer processes that constitute the photocycle of GFP. Our results demonstrate the utility of multiple-pulse spectroscopy: with traditional time-resolved spectroscopy, a reaction path is predetermined once it has been initiated. By the application of multiple-pulse sequences, reaction paths can actively be influenced and controlled, affording a powerful way to extract information that would otherwise remain unavailable.

We thank Profs. Silvia Völker and Holger Lill for critically reading the manuscript. J.T.M.K is supported through a VIDI grant by the Earth and Life Sciences Council of the Netherlands Organization for Scientific Research (NWO-ALW). D.S.L. is grateful to the Human Frontier Science Project Organization for granting a long-term fellowship. J.T.M.K. and M.V. were supported by the Organization for Fundamental Research on Matter (FOM). J.J.v.T. is a Royal Society University Research Fellow.

1. Tsien, R. Y. (1998) *Annu. Rev. Biochem.* **67,** 509–544.
2. Chattoraj, M., King, B. A., Bublitz, G. U. & Boxer, S. G. (1996) *Proc. Natl. Acad. Sci. USA* **93,** 8362–8367.
3. Yang, F., Moss, L. G. & Phillips, G. N. (1996) *Nat. Biotechnol.* **14,** 1246–1251.
4. van Thor, J. J., Gensch, T., Hellingwerf, K. J. & Johnson, L. N. (2002) *Nat. Struct. Biol.* **9,** 37–41.
5. Creemers, T. M. H., Lock, A. J., Subramaniam, V., Jovin, T. M. & Volker, S. (1999) *Nat. Struct. Biol.* **6,** 557–560.
6. Brejc, K., Sixma, T. K., Kitts, P. A., Kain, S. R., Tsien, R. Y., Ormo, M. & Remington, S. J. (1997) *Proc. Natl. Acad. Sci. USA* **94,** 2306–2311.
7. Palm, G. J., Zdanov, A., Gaitanaris, G. A., Stauber, R., Pavlakis, G. N. & Wlodawer, A. (1997) *Nat. Struct. Biol.* **4,** 361–365.
8. Lossau, H., Kummer, A., Heinecke, R., Pollinger-Dammer, F., Kompa, C., Bieser, G., Jonsson, T., Silva, C. M., Yang, M. M., Youvan, D. C., *et al.* (1996) *Chem. Phys.* **213,** 1–6.
9. Winkler, K., Lindner, J. R., Subramaniam, V., Jovin, T. M. & Vöhringer, P. (2002) *Phys. Chem. Chem. Phys.* **4,** 1072–1081.
10. Crameri, A., Whitehorn, E. A., Tate, E. & Stemmer, W. P. C. (1996) *Nat. Biotechnol.* **14,** 315–319.
11. Gai, F., McDonald, J. C. & Anfinrud, P. (1997) *J. Am. Chem. Soc.* **119,** 6201–6202.
12. Changenet-Barret, P., Choma, C., Gooding, E., DeGrado, W. & Hochstrasser, R. M. (2000) *J. Phys. Chem. B* **104,** 9322–9329.
13. Logunov, S. L., Volkov, V. V., Braun, M. & El-Sayed, M. A. (2001) *Proc. Natl. Acad. Sci. USA* **98,** 8475–8479.
14. Larsen, D. S., Papagiannakis, E., van Stokkum, I. H. M., Vengris, M., Kennis, J. T. M. & van Grondelle, R. (2003) *Chem. Phys. Lett.* **381,** 733–742.
15. Larsen, D. S., Vengris, M., van Stokkum, I. H. M., van der Horst, M. A., de Weerd, F. L., Hellingwerf, K. J. & van Grondelle, R. (2004) *Biophys. J.* **86,** 2538–2550.
16. Larsen, D. S., Vengris, M., van Stokkum, I. H. M., van der Horst, M. A., de Weerd, F. L., Hellingwerf, K. J. & van Grondelle, R. (2004) *Biophys. J.* **87,** 1858–1872.
17. Vengris, M., van Stokkum, I. H. M., He, X., Bell, A. F., Tonge, P. J., van Grondelle, R. & Larsen, D. S. (2004) *J. Phys. Chem. A* **108,** 4587–4598.
18. van Stokkum, I. H. M., Larsen, D. S. & van Grondelle, R. (2004) *Biochim. Biophys. Acta* **1657,** 82–104, and erratum (2004) **1658,** 262.
19. van Thor, J. J., Pierik, A. J., Nugteren-Roodzant, I., Xie, A. H. & Hellingwerf, K. J. (1998) *Biochemistry* **37,** 16915–16921.
20. Gradinaru, C. C., Kennis, J. T. M., Papagiannakis, E., van Stokkum, I. H. M., Cogdell, R. J., Fleming, G. R., Niederman, R. A. & van Grondelle, R. (2001) *Proc. Natl. Acad. Sci. USA* **98,** 2364–2369.
21. Striker, G., Subramaniam, V., Seidel, C. A. M. & Volkmer, A. (1999) *J. Phys. Chem. B* **103,** 8612–8617.
22. Ruhman, S., Hou, B., Freidman, N., Ottolenghi, M. & Sheves, M. (2002) *J. Am. Chem. Soc.* **2002,** 8854–8858.
23. Cormack, B. P., Valdivia, R. A. & Falkow, S. (1996) *Gene* **173,** 33–38.
24. Wiehler, J., Jung, G., Seebacher, C., Zumbusch, Z. & Steipe, B. (2003) *ChemBioChem* **4,** 1164–1171.
25. Lill, M. A. & Helms, V. (2002) *Proc. Natl. Acad. Sci. USA* **99,** 2778–2781.
26. Sham, Y. Y., Muegge, I. & Warshel, A. (1999) *Proteins* **36,** 484–500.
27. Arlt, T., Schmidt, S., Kaiser, W., Lauterwasser, C., Meyer, M., Scheer, H. & Zinth, W. (1993) *Proc. Natl. Acad. Sci. USA* **90,** 11757–11761.